Pure and Applied Geophysics manuscript No.
(will be inserted by the editor)

Ambient seismic noise tomography of a loess high bank at Dunaszekcső (Hungary)

Gyöngyvér Szanyi · Zoltán Gráczer · Erzsébet Győri · Zdeněk Kaláb · Markéta Lednická

Published online: 11 May 2016

Abstract Loess high banks along the right side of the Danube in Hungary are potential subjects to landslides. Small scale ambient seismic noise tomography was used at the Dunaszekcső high bank. The aim of the study was to map near surface velocity anomalies since we assume that the formation of tension cracks – which precedes landslides – are represented by low velocities. Mapping Rayleigh wave group velocity distribution can help to image intact and creviced areas and identify the most vulnerable sections. The study area lies at the top of the Castle Hill of Dunaszekcső, which was named after *Castellum Lugio*, a fortress of Roman origin. The presently active head scarp was formed in April 2011, our study area was chosen to be at the surroundings of it. Cross-correlation functions of ambient noise recordings were used to retrieve the dispersion curves which served as the input of the group velocity tomography. Phase cross-correlation and time-frequency phase weighted stacking was applied to calculate the cross-correlation functions. The average Rayleigh wave group velocity at the loess high bank was found to be 171 ms^{-1}. The group velocity map at 0.1 s period revealed a low-velocity region, whose location coincides with a highly creviced area, where slope failure takes place along a several metre wide territory. Another low velocity region was found, which might indicate a previously unknown loosened domain. The highest velocities were observed at the supposed remnants of *Castellum Lugio*.

Keywords seismic interferometry · ambient noise · group velocity · tomography · landslide · high bank

Gy. Szanyi* · Z. Gráczer · E. Győri
MTA CSFK GGI Kövesligethy Radó Seismological Observatory
Meredek st. 18., H-1112 Budapest, Hungary
E-mail: *szanyi.gyongyver@csfk.mta.hu

Z. Kaláb · M. Lednická
Institute of Geonics, Academy of Sciences of the Czech Republic
Studentská str. 1768, CZ-708 00 Ostrava, Czech Republic

1 Introduction

In near surface seismic studies most frequently longitudinal waves are used because execution and evaluation of the measurements are relatively simpler than in case of using shear waves. In addition, longitudinal waves usually have higher dominant frequency and they are also suitable for applications which are related to soil humidity, e.g. monitoring of changes in the level of water table. Despite all of the above mentioned benefits, recently developed shear wave based methods have been gaining importance in shallow seismic studies. One of the advantages of using shear waves is that under favourable conditions much higher resolution can be achieved than in the case of using P waves. The v_P/v_S ratio in hard rocks is about $\sqrt{3}$, but in near surface soft material it can reach values over 20 (Barton, 2007), which means that in shallow, unconsolidated sediments, shear waves travel much slower, than longitudinal waves, therefore their wavelengths are shorter, resulting in higher resolving power despite the higher frequency content of P waves.

Small scale P wave studies often have limited capability of detecting geological changes, because the watertable might be the strongest reflector in the upper few meters. However, water saturation does not have a great influence on shear wave velocities (Barton, 2007), therefore they are barely affected by the watertable allowing the recognition of geological changes. Being almost independent from water saturation also means

that shear wave velocities have almost the same values after dry or wet weather periods, thus velocities measured at various times are comparable.

Mapping shear wave velocities in a relatively simple manner and at a low cost is challenging even today. From the point of view of measurement one of the most feasible and cost-effective methods is seismic interferometry which utilises ambient seismic noise. It is possible to implement it with only two instruments, which are easy to install and which can be placed even on streets in urban areas or industrial sites. Thus ambient noise tomography can be used where other geophysical methods might not be applicable. In addition, the measurement time depends on station distance, the shorter the distance, the lesser the time required (Sabra et al, 2005b; Gouedard et al, 2008). This method can be equally well used on continental (Yang et al, 2007; Bensen et al, 2009), regional (Szanyi et al, 2013; Ren et al, 2013; Dias et al, 2015), local (Renalier et al, 2010; Stankiewicz et al, 2012) and engineering-geotechnical scale (Picozzi et al, 2009; De Nisco and Nunziata, 2011; Pilz et al, 2012, 2014).

One of the key assumptions of the noise correlation method is that the noise sources are randomly distributed in all directions (e.g. Shapiro and Campillo, 2004). However, recent studies have shown (Yang and Ritzwoller, 2008; Picozzi et al, 2009) that this method can be used even in case of non-uniform distribution of noise sources. According to Picozzi et al (2009) only 30 min of recording time is sufficient for high frequency (5-14 Hz) measurements at engineering-geotechnical scale. Pilz et al (2014) have shown that ambient noise tomography can be used in the case of significant topographic relief, however traveltimes may change when the difference in height is larger than the wavelength or the penetration depth (Pilz et al, 2014).

Considering the results of Pilz et al (2014), we assumed that ambient noise tomography is applicable at such an asymmetrical environment as a high bank, which is very common along the Danube in Hungary. In these areas weakly consolidated loess sequences form steep slopes, which are prone to slide. Although landslides have localised impact, they represent a significant natural hazard as the Hungarian high bluffs are presently active and landslides occur from time to time. In particular the high bank at Dunaszekcső is part of the village, even houses were built on the currently slumping block.

In this paper we aim at mapping near surface Rayleigh wave group velocities at an active mass movement in Dunaszekcső. The study area is a strongly asymmetrical high bank environment, bounded by a precipice of landslide origin. We assume the sliding event to be preceded by the formation of tension cracks, which appear as low velocity zones. Therefore we intend to image velocity contrasts between the intact and the creviced areas.

2 Study Area

At the right side of the Danube south of Budapest six active high bank sections can be found along the Hungarian part of the river (Kovács et al, 2015). The Dunaszekcső high bank, located approximately 20 km north of the Hungarian-Croatian border, is one of the most active bluffs of Hungary with recurring sliding events. Since the middle of the last century major landslides have been observed every 10 to 20 years (Kraft, 2011; Kovács et al, 2015). The high bank is approximately 15 km long and it has been intensively studied for decades by means of geomorphological (Moyzes and Scheuer, 1978; Újvári et al, 2009; Kraft, 2011; Lóczy, 2015), geotechnical (Moyzes and Scheuer, 1978), geodetical (e.g. Bugya et al, 2011; Bányai et al, 2014) and seismological methods (Hegedűs, 2008).

The studied area is located at the southern part of the high bank. It covers an approximately 100 m×80 m large territory on top of the Castle Hill (Dunaszekcső). The head scarp runs in approximately north-south direction in its eastern part (Fig. 1). Most of the above mentioned studies examined the Castle Hill, however seismic tomography was not carried out on our study area. East to the head scarp a potential future fracture system was mapped by geoelectrical measurements (Szalai et al, 2014b) and pressure probe method (Szalai et al, 2014a). At Castle Hill and at its northern neighbour – the Szent János Hill – geodetic monitoring of surface movements by GPS measurements has been performed and deformations have been measured by borehole tiltmeters (Mentes et al, 2012; Bányai et al, 2014).

Along the Danube, archaeological sites give an opportunity to estimate the river bank retreat. The frontier (limes) of the Roman Empire ran along the Middle Danube, where fortresses and watchtowers were built for defence (Visy, 2003). Reconstruction of the ground plans and using historical maps revealed that in some cases major parts of the fortresses have been destroyed by landslides. On the basis of the archaeological evidences a rate of approximately 1-2 m per 100 years on average was ascertained for the river retreat (Kovács et al, 2015). This could have been higher in active undercutting periods (2-10 m per 100 years) and even higher over the last 100 years, when human activity might have increased the retreat up to above 10 m per 100 years (Lóczy et al, 1989).

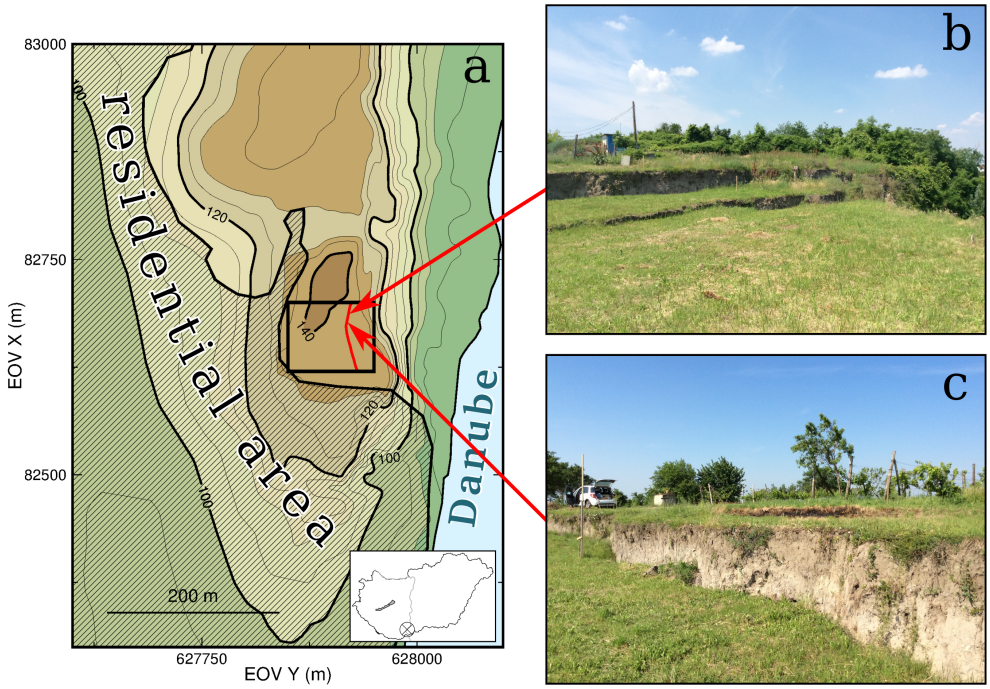

Fig. 1 a) Elevation map of the study area and its surroundings. Coordinates are given in the Hungarian EOV coordinate system. The village of Dunaszekcső lies at the foot of the Castle Hill and the Danube flows east to it. The black rectangle denotes the study area, where the red line indicates the head scarp. **b)** and **c)** Photos of the head scarp at its northern part. The failure process affects a several meter wide area. The photos were taken during the June 2015 measurement campaign, when the shown scarp was approximately 1.6 m high.

Sliding events are a result of different morphological and hydrological circumstances; elevated groundwater level and increased precipitation after a dry period are presently considered as main triggering factors (Bányai et al, 2014; Kovács et al, 2015).

When studying the Castle Hill, it is important to take into consideration that *Castellum Lugio*, an ancient fort of Roman origin lied at the top of the hill, with dimensions of 150 metres in north-south direction and approximately 180 metres in east-west direction (Visy, 2015 pers.com.). The castle was rebuilt either by the Romans in the 4th century or by the Turks during the Turkish occupation in Hungary, as it is also known that in the 16-18th century, a fort stood at the top of the hill (Visy, 2015 pers.com.). Due to the continuous landsliding its eastern side is being destroyed, only 81 m wide territory remained of the previous fort. The stones of the castle were reused at local constructions, currently no remains of walls can be seen on the surface. However, the possible buried remnants can affect the results of any geophysical measurements carried out on the top of the Castle Hill. Unfortunately detailed archaeological excavations of the fort have not been conducted (Visy, 2003), therefore only a manuscript map of the walls still visible in the early 20th century and a few historical documents can possibly help in the interpretation of the results of geophysical surveys in the area.

The Castle Hill's highest point is approximately 60 m above the mean water level of the Danube (82-83 m a.s.l.). The top of the hill is almost flat, however, it is slightly sloping to the east, towards the Danube. Castle Hill is bounded by steep slopes in every direction. The village of Dunaszekcső lies southwards and westwards at the foot of the studied part of the hill, however, there are no nearby houses northwards (Fig. 1).

A vertical loess wall of 20-30 m rises above the 10-20 m high slopes of reworked sediments of past landslides and fluvial deposits of the Danube (Újvári et al, 2009; Kovács et al, 2015). The floodplain is very narrow, therefore, despite the protection measures, the river repeatedly undercuts the slopes during flood events. The bluff consists of Pleistocene sediments. The younger loess series on top includes brown paleosol levels. Its thickness is 40 m on average and it is prone to collapse. The underlying series of sandy silts and clays contain brown, red and green paleosol levels. This older Pleistocene sequence is much more consolidated and its thickness varies from 5 to 15 m (Kraft, 2011).

Development of tension cracks and movements along the head scarp are probably a result of reduced cohesive strength due to previous sliding and slumping events.

The last major movement occurred in 2008, when a 240 m long area parallel to the Danube slid down 4 to 10 m vertically with lateral displacement up to 4 m (Kraft, 2011). The width of the slumping block was 30 m at its greatest extent. The main movement involved approximately 550,000 m^3 rock mass and lasted for hours. The affected area has come to temporary rest after 3 days. A total of 520 m long and a maximum of 240 m wide area was involved in the process. In April 2011 a new rupture surface was formed, since then smaller movements have been taking place along it.

Between our two measurement campaigns in October 2014 and June 2015 the slump block slid down several tens of centimetres. At the northern end of the head scarp, the topographic relief increased from approximately 0.9 m to 1.6 m, while at the southern part the sliding was somewhat greater, the height of the scarp increased from approximately 0.6 m to 1.6 m. In October 2014 the rupture surface was limited to a narrow strip, while in June 2015 at the northern section of the scarp several steps were to be seen in a few metres wide area (Fig. 1).

3 Data Acquisition

In October 2014, ambient noise measurements were performed at an approximately 100 m×80 m area on the Castle Hill using 3 Lennartz LE-3D/5s seismometers with Guralp CMG-EAM digitisers. Measuring arrangement was designed in order to be able to apply different noise based methods such as Horizontal to Vertical Spectral Ratio (e.g. Nakamura, 2000), Microseismic Sounding Method (MSM) (e.g. Gorbatikov et al, 2004) and seismic interferometry. 31 measurement points were marked in 5 rows, perpendicular to the Danube (Fig. 2a). The Microseismic Sounding Method needs a base station, which was deployed at the centre of the study area and recorded continuously. Interstation distance between the simultaneously recording instruments varied from 11 m to 89 m. For better coupling between the instruments and soil, granite plates were placed under the sensors.

Precise positions of measurement points were determined using Real Time Kinematics (RTK) technology, which is a differential Global Navigation Satellite System technique. It provides high positioning performance allowing cm-scale precision (Hofmann-Wellenhof et al, 2001).

After the preliminary processing of the noise recordings of October 2014, additional measurements were carried out in June 2015 to improve the tomographic resolution (Fig. 2a). Five Lennartz LE-3D/5s seismometers were utilised with three Guralp CMG-EAM and two GAIA Vistec digitisers. Station-to-station distances up to 101 m were used. The resolution test based on the first campaign's data showed that paths parallel to the Danube are needed, therefore station pairs were installed predominantly in north-south direction. Attention has been paid to make measurements parallel to the head scarp as well and to have paths which do not cross the trace of the scarp, but are close to it.

Before the measurements in October 2014, recording parameters were tested on a sedimentary site to decide minimum recording time and necessary sampling frequency. Based on the SNR values of the cross-correlation functions the test results indicated that a recording time of 45 minutes at 100 Hz frequency is suitable for dispersion curve determination at the distance range from 10 to 100 m. These recording parameters and GPS timing were used during both measurement campaigns.

Between October 2014 and June 2015 a several tens of centimetres sliding along the head scarp occurred, therefore control measurement was made during the second campaign to verify the stability of the dispersion curves. The same measurement was used to verify instrument pair configuration compatibility in practice as well.

Location of the station pair for the control measurement was selected after processing the noise recordings of the first measurement campaign. It was noteworthy that group velocities associated with a particular head scarp crossing path were significantly higher than the group velocities for the other station pairs (see Fig. 4a). Therefore, the control measurement served to check the reliability of that measurement as well. Four of the instruments were used, among them two were used in the first campaign as well, therefore these were installed at the same points with identical parameters (measurement time, sampling frequency) as previously. The other two instruments were Lennartz LE-3D/5s seismometers equipped with GAIA Vistec digitisers, which measured in the immediate vicinity of the first control line. The dispersion curves obtained from the various instrument configurations (Guralp-Guralp, Guralp-GAIA, GAIA-GAIA digitiser pairs) were in good agreement, thus cross-correlation computation was carried out between every possible station pair, regardless the type of the used digitiser. The control measurement resulted in very similar dispersion curves to that of the first campaign's, thus the stability of the dispersion curve was confirmed and high velocities associated with the control measurement's path were accepted as reliable values.

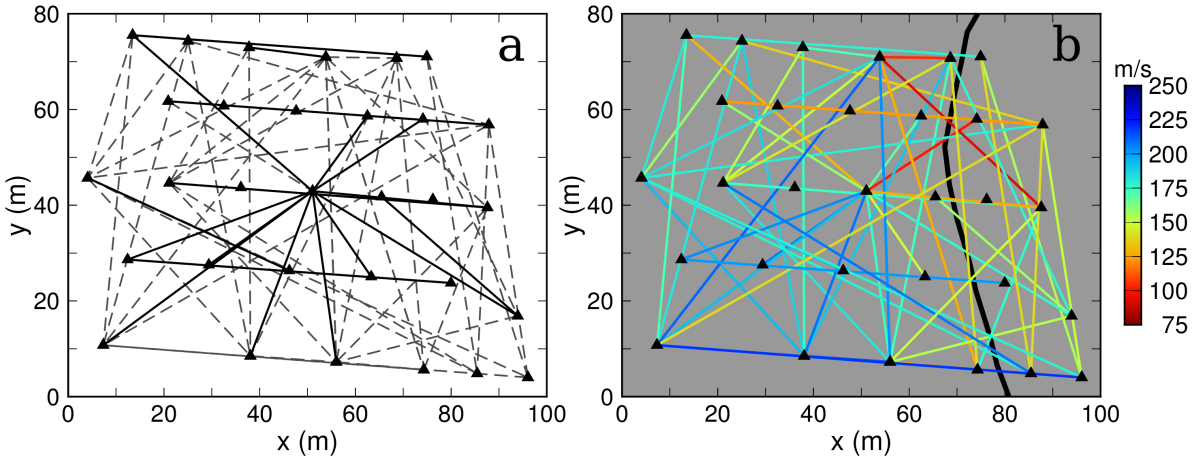

Fig. 2 a) Paths belonging to the two measurement campaigns. Coordinates are given in local coordinate system. The origin is at 627850 m and 82620 m in the EOV system. *Triangles*: instrument locations. *Continuous lines*: first campaign in October 2014, where station configuration was designed to use several ambient noise based methods. *Dashed lines*: second campaign in June 2015 to obtain additional paths to improve tomographic resolution. **b)** The measured group velocities in ms^{-1} for each path at 0.1 s period. The thick black line marks the head scarp.

4 Correlation Analysis and Stacking

The empirical Green's function for the structure between a station pair can be obtained as the negative time derivatives of the cross-correlation functions of simultaneously recorded seismograms predominantly containing ambient noise (Sabra et al, 2005a). However, for narrow bandwidth signals it is an acceptable approximation to use the cross-correlation function as an estimate of the Green's function (Sabra et al, 2005a). In this paper cross-correlation functions were used to obtain the dispersion curves and estimate Rayleigh wave group velocities.

In order to retrieve the dispersion curves, the processing procedure of ambient noise data consists of four main steps (Bensen et al, 2007): 1) data preparation, 2) cross-correlation and stacking, 3) measurement of dispersion curves and 4) quality control. Different methods were tested for the processing steps of correlation analysis and stacking and the best combination of them was selected to retrieve the cross-correlation functions and the dispersion curves.

Data preparation begun with removing the mean and trend followed by frequency filtering. Since our aim was to investigate the near surface structures, only high frequencies were of interest. Therefore a high-pass filter with corner frequency of 3 Hz was used. Thereafter the continuous recordings were cut into 45 s long segments, which was followed by time-domain normalisation and cross-correlation.

Bensen et al (2007) tested different time-domain normalisation methods and found that running absolute mean normalisation and one-bit normalisation gives the best signal-to-noise ratio (SNR) when computing the cross-correlation function. Based on their results we have chosen to apply one-bit normalisation.

The second phase of the ambient noise processing procedure is the cross-correlation computation and stacking of correlation functions. In the literature generally conventional correlation (which is based on the products of the amplitudes) is used to obtain correlation functions (e.g. Campillo and Paul, 2003; Bensen et al, 2007), thus this method was one possible candidate for our computations.

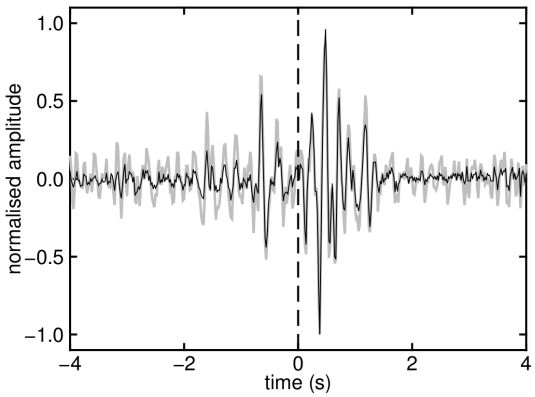

Fig. 3 Cross-correlation functions computed using different normalisation and stacking techniques. The *gray line* shows the correlograms obtained using one-bit normalisation, conventional cross-correlation, and linear stacking, while the overplotted *black line* shows the cross-correlation function of phase correlation and time-frequency phase weighted stacking (Schimmel and Gallart, 2007). Both correlograms are amplitude normalised. The presented cross-correlation function is not symmetric, which indicates uneven noise source distribution.

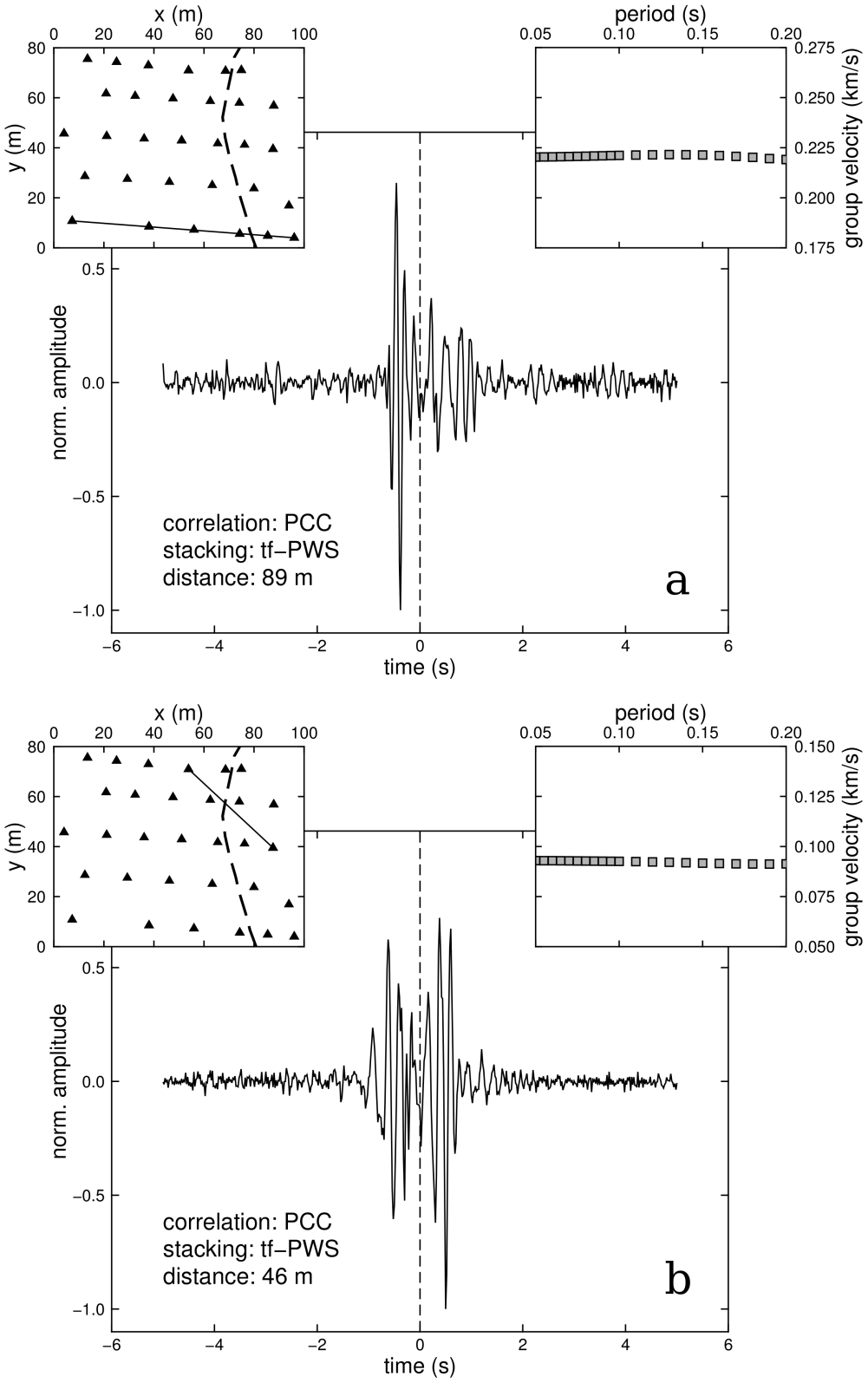

Fig. 4 a) The obtained cross-correlation function for a long path. The cross-correlation function was calculated using the phase cross-correlation method and time-frequency phase weighted stacking. Upper left corner: location map of measurements and the path for which the cross-correlation function was calculated. *Triangles* mark station locations while the *dashed line* shows the head scarp. The interstation distance was 89 m. Upper right corner: dispersion curve retrieved from the cross-correlation function using the multiple filter technique. **b)** Same as in a) but for a shorter path that crossed the northern part of the head scarp. Interstation distance was 46 m.

Seeking better cross-correlation functions, we tested the phase cross-correlation (PCC) method (Schimmel, 1999) as well. PCC has been shown to improve the SNR of the cross-correlation function (Schimmel, 1999; Schimmel et al, 2011). This method is more sensitive to waveform similarity and less sensitive to large amplitude phenomena than the conventional cross-correlation and it does not require time-domain normalisation (Schimmel et al, 2011). Therefore we omitted the normalisation step when PCC was applied.

The stacking of the cross-correlation functions is an important tool to improve the SNR, thus two types of stacking techniques have been tested: 1) standard linear stacking, which is used in most of the ambient noise tomography studies (e.g. Sabra et al, 2005a; Shapiro et al, 2005; Yang et al, 2007; Cho et al, 2007; Bensen et al, 2009) and 2) time-frequency phase weighted stacking (tf-PWS) described by Schimmel and Gallart (2007), which has been applied in some recent ambient seismic noise tomography studies (e.g. Ren et al, 2013; Dias et al, 2015).

Various combinations of the previously described processing steps have been used to calculate the cross-correlation functions. We compared the SNR ratio of the obtained cross-correlation functions and concluded that phase correlation with phase weighted stacking led to the best SNR. Fig. 3 shows an example for a cross-correlation function computed with conventional cross-correlation combined with linear stacking and the PCC combined with tf-PWS. It can be seen that the SNR is higher in case of using the PCC together with tf-PWS. Examples of the cross-correlation functions and corresponding dispersion curves are shown in Fig. 4.

The obtained cross-correlation functions were rarely symmetric (e.g. Fig. 3), indicating that the sources of ambient noise are non-uniformly distributed azimuthally, therefore we have performed noise directionality analysis to examine the azimuthal distribution of ambient noise sources and to identify the direction of energy propagation. Following the method by Lin et al (2007) we have compared the SNR of the positive and negative correlation lags. The SNR of both lags were computed separately and multiplied by the root square of the interstation distance to compensate for geometrical spreading. For each station pair two lines with opposite direction were drawn at both stations, representing the causal and acausal lags (Fig. 5). Their lengths are proportional to the above mentioned SNR related values. The azimuths of the lines correspond to the station-station line. Lines originating from the stations show the direction of energy propagation.

The directionality analysis shows that energy is propagating from all directions, however the main energy flux is coming from south and west of the study area. Considering the location map (Fig. 1) it can be assumed that the main contributor to the signals of the correlograms is the residential area of Dunaszekcső.

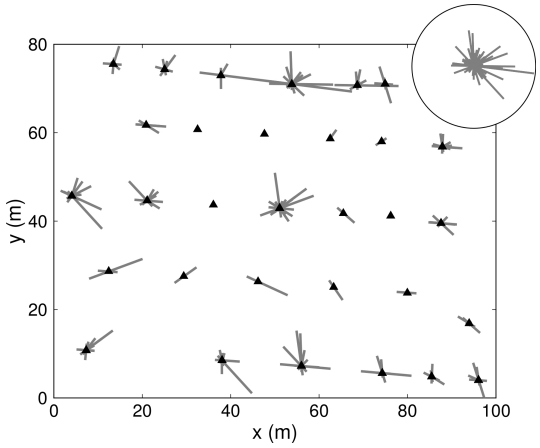

Fig. 5 Directionality analysis of noise sources. Signal-to-noise ratio was calculated for every cross-correlation function for both correlation lags. For the sake of clarity at both stations of each station pair two lines were drawn representing the two sides of the cross-correlation function. Their lengths are proportional to the SNR multiplied by the square root of the interstation distance. The azimuths of the lines are defined by the station-station line. Lines originating from the stations show the direction of energy propagation. *Inset:* Summary of the directions of energy propagation for every measurement.

5 Measuring Group Velocities

A dispersion curve describes velocities of seismic waves of different periods. We have studied cross-correlation functions of vertical component noise recordings, therefore the measured group velocity dispersion curves correspond to Rayleigh waves.

Group velocity dispersion curves were obtained using the *do_mft* software of Herrmann and Ammon (2002). It applies the multiple filter technique (Dziewonski et al, 1969; Herrmann, 1973), which utilises a Gaussian filter to isolate a wave package around the central frequency (Ammon, 2001) using the operator $\exp\left(-\alpha(f-f_c)^2/f_c^2\right)$ (Herrmann, 1973; Herrmann and Ammon, 2002), where f_c is the central frequency. The optimal value of filter width (α) depends on station-to-station distance in case of ambient noise based cross-correlation functions and it is determined empirically in practice. Choosing the α patameter means a compromise between resolution in the time and frequency domains, larger values of α improve the resolution in the frequency domain but deteriorate resolution in the time domain (Levshin et al, 1989). Based on Ammon (2001) the width of the Gaussian filter was chosen to minimise

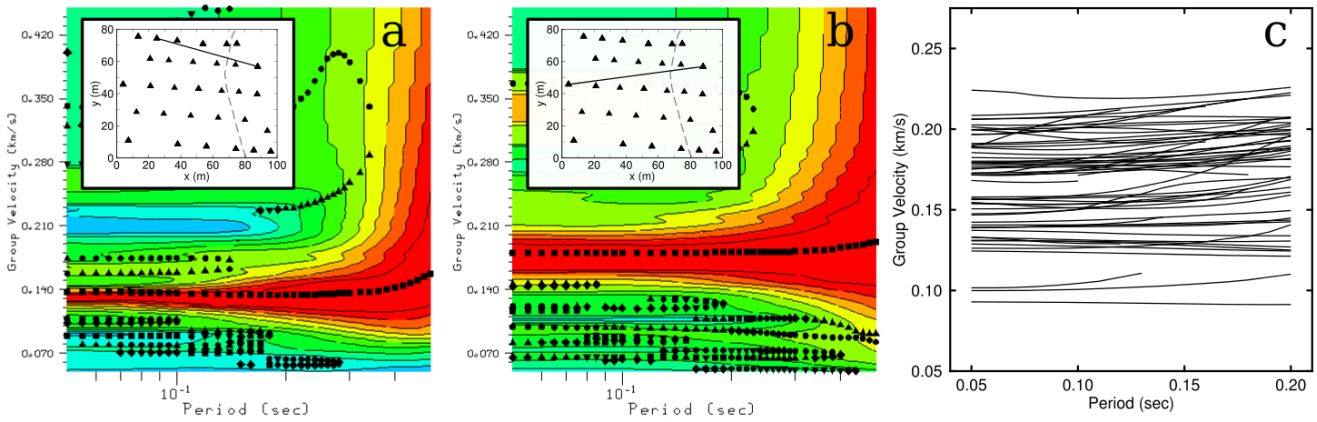

Fig. 6 a-b) Multiple filter analysis plots for the station pairs shown in the insets. The colouring represents the spectral amplitudes of the multiple filtered cross-correlation functions. Warm colours show higher amplitudes. Squares in the red area correspond to the largest amplitude for each period and indicate the group velocity dispersion curve, while other symbols display the local maxima. **c)** Rayleigh wave dispersion curves used for tomographic computations.

the area of the fundamental mode in the multiple filter analysis (MFA) plot. After testing different filter width values $\alpha = 1$ was chosen for dispersion curve measurements.

Reliable dispersion measurements for a given period require an interstation spacing of at least one wavelength (Luo et al, 2015), which was considered during selection of the reliable paths. In most cases, the cross-correlation function was not symmetric, indicating uneven distribution of noise sources as described in the previous section. Therefore, both the causal and acausal parts of the correlograms and the average of the two sides ('symmetric signal') were processed. Only clearly delineated dispersion curves along well defined ridges in the MFA contour plot were selected (Fig. 6a,b). Dispersion curves with sudden jumps in group velocities or without clear maximum on the MFA plot were rejected. Out of 136 cross-correlation functions 62 yielded an acceptable dispersion curve.

Group velocities corresponding to different azimuths can be used to examine anisotropic properties of an area. At the investigated area the presence of planar cracks along the head scarp suggests that azimuthally dependent velocities would emerge. Therefore, the obtained group velocities were used to detect possible anisotropy. First, azimuth versus group velocity (Fig. 7a), then the distribution of estimated traveltimes as a function of the distance and the azimuth between each station pair was plotted (Fig. 7b). Fig. 7 shows that the observed traveltime variations are mainly dependent on the distance, neither the group velocities nor the delay times seem to vary systematically with azimuth.

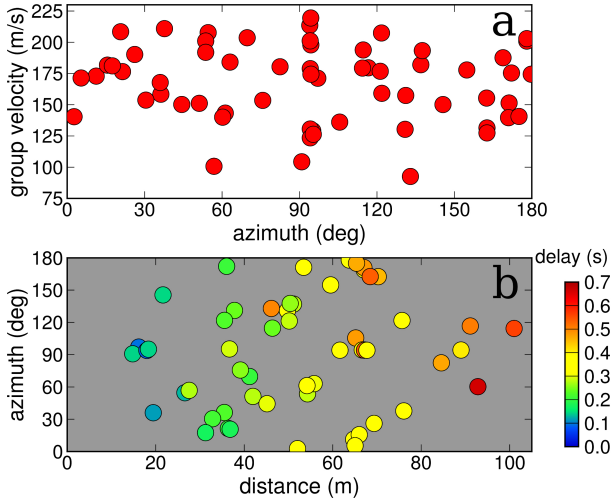

Fig. 7 a) Azimuth versus group velocity **b)** Distribution of estimated traveltimes as a function of distance and azimuth between each station pair.

6 Tomography

The aim of our tomographic computations was to estimate the 2D Rayleigh wave group velocity distribution in the investigated area. Input parameters for this problem were 1) traveltimes determined from the interstation distances and corresponding group velocities and 2) locations of measurement points. To solve the tomographic problem, a 2D iterative, linearised method (e.g. Yanovskaya et al, 1998; Barmin et al, 2001) was used and ray-curvature was neglected.

The dispersion curves were almost flat in the period range of interest (see Fig. 6c), therefore shear wave velocity versus depth inversion was not carried out. Tomographic computations were performed only for 0.1 s period.

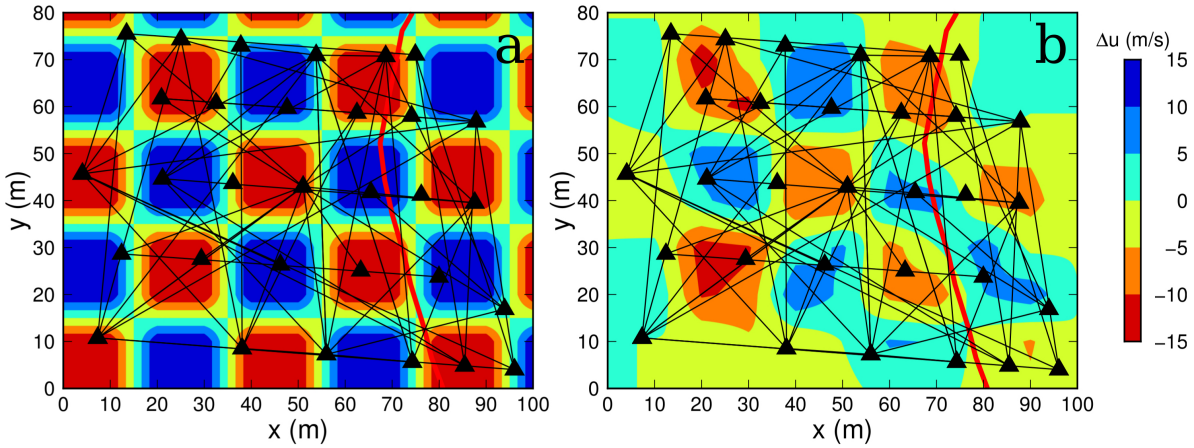

Fig. 8 The checkerboard test for an anomaly size of 20 m×20 m with the ray path coverage in local coordinate system. *Triangles* mark station locations while *red line* denotes the head scarp. **a)** Checkerboard model. **b)** The inverted checkerboard.

To determine depth range whose velocities affect the group velocity distribution we must compute the sensitivity kernel for the given period. Based on the literature typical values of Poisson's ratio for near surface loess sequences are between 0.25 and 0.38 (e.g. Danneels et al, 2008; Wang et al, 2012). Using homogeneous half space approximation (e.g. Lay and Wallace, 1995) the Rayleigh wave velocity is slightly less than the shear velocity for the above mentioned Poisson's ratios ($v_{Rayleigh}$=0.92-0.94 v_S). Sensitivity kernel was computed using the average of the measured group velocities (167 ms^{-1}), the relationship $v_{Rayleigh}$=0.93v_S, an average Poisson's ratio of 0.315 and an approximate loess density of 1.6 g/cm^3 (e.g. Danneels et al, 2008; Gergova et al, 1995). The result shows that the Rayleigh waves of 0.1 s period sample the upper 4 m on average.

The study area is basically flat and it is slightly sloping towards the Danube. The most striking feature is the head scarp, which was approximately 1.6 m high during the second measurement campaign in June 2015. An accurate description of the velocity structure should include this complex topography as well. However, according to Pilz et al (2014) the topographic relief can be neglected if it is small compared to the studied wavelengths, which is between approximately 8 and 24 m in our case depending on the velocity. Therefore the height difference between the stable block and the slumping block was not taken into account when defining the velocity grid. Velocities were given on an equally spaced Cartesian grid and bilinear interpolation was used to calculate velocities between the grid points. The grid spacing was set to 10 m.

The linearised tomographic inverse problem can be written as

$$\mathbf{d} = \mathbf{Gm} \tag{1}$$

where $\mathbf{d}$ is the data residual vector, whose elements are the difference between the measured and computed group traveltimes. The $\mathbf{m}$ model vector represents the slowness (i.e. inverse of group velocity) perturbation from the reference slowness model. $\mathbf{G}$ is the kernel matrix. The size of $\mathbf{d}$ vector equals to the number of obtained dispersion curves at a specific period, while the length of the model vector is defined by the number of grid points of the velocity field representation.

We assumed that the observational errors of group velocities at a given period are equal therefore data weighting was not applied. As we are interested in the eventual abrupt change in velocity field related to the head scarp, the inverse problem was regularized only by penalizing the slowness perturbation, but a distinct spatial smoothing operator (e.g. Laplacian) was not used. Taking into account the above mentioned considerations we can write the misfit function as

$$\mathbf{\Phi}(\mathbf{m}) = (\mathbf{d} - \mathbf{Gm})^T(\mathbf{d} - \mathbf{Gm}) + \epsilon^2\mathbf{m}^T\mathbf{m} \tag{2}$$

where ϵ^2 is the damping parameter (Menke, 1989). The tomographic inverse problem can be solved by minimizing this misfit function. The solution $\hat{\mathbf{m}}$ can be given as

$$\hat{\mathbf{m}} = (\mathbf{G}^T\mathbf{G} + \epsilon^2\mathbf{I})^{-1}\mathbf{G}^T\mathbf{d} \tag{3}$$

where $\mathbf{I}$ is the identity matrix (Menke, 1989).

Based on the trade-off curve between model perturbation and data misfit, the damping parameter was set to $\epsilon = 2.0$. The starting velocity model was a constant velocity field of 167 ms^{-1}, which is equal to the average group velocity calculated from all dispersion curves at 0.1 s period. The initial rms was 0.065 s which decreased to 0.031 s. The iteration process ended after 4 iteration steps, when the rms reduction between two successive steps was less than 5% of the initial rms.

To be able to reliably interpret the tomographic results, it is important to test the spatial resolution, therefore checkerboard tests were performed. The checkerboard was defined as adjacent groups of gridpoints with ±10% velocity anomalies. It is assumed that if the original anomalies of the checkerboard can be recovered, then a real velocity anomaly of similar size, location and amplitude could be resolved. Lévěque et al (1993) has shown that a checkerboard test only represents the resolution for certain anomaly sizes and may not be able to resolve larger scale anomalies. Using different block sizes in checkerboard tests reduces the risk of misinterpretation (e.g. Bijwaard et al, 1998). Therefore recovery ability was examined by checkerboard tests for different anomaly sizes from 10×10 m to 40×40 m. An example of the tests is shown in Fig. 8.

To supplement the checkerboard tests, error bounds for the tomographic problem were calculated using the bootstrap method (Efron, 1979; Tichelaar and Ruff, 1989). The key concept in bootstrapping is to resample the original data set to form a large number of new data sets, whose size is set equal to that of the original data set. Therefore the compiled bootstrap samples may contain a certain original datum more than once. During the error estimation 1000 bootstrap inversions were executed. The standard deviation of the obtained velocities is estimated by the standard error of the inversion of the ensemble of the bootstrap samples for each grid point. In regions without a crossing path, the uncertainty is zero as it only has meaning where there is path coverage (see Fig. 9).

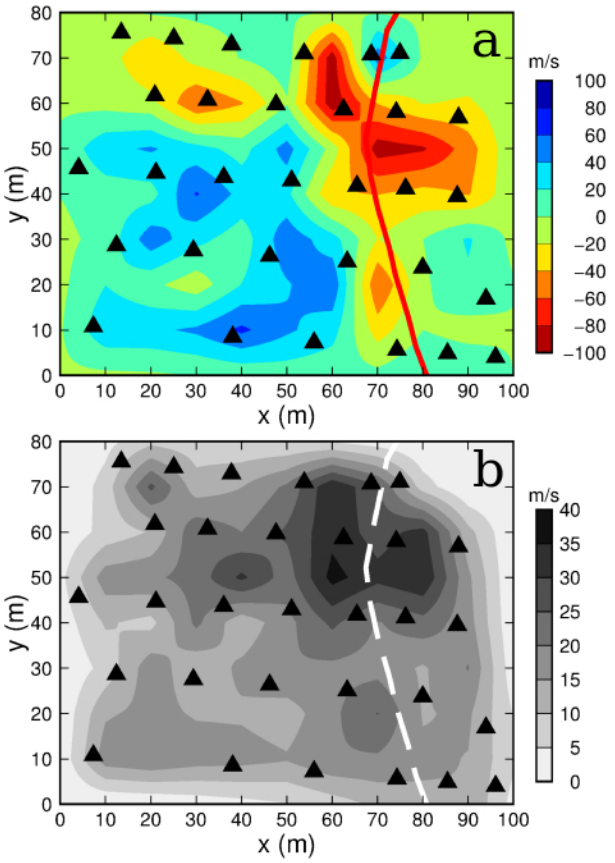

Fig. 9 a) Rayleigh wave group velocity distribution for the study area in local coordinate system at 0.1 s period. Group velocities in ms^{-1} are shown relative to the average value (171 ms^{-1}). *Triangles* mark measurements points while the *red line* denotes the head scarp. **b)** Velocity standard deviation computed by bootstrapping. Velocities are in ms^{-1}.

7 Results and Discussion

Noise measurements were carried out on an active landslide at Dunaszekcső. The obtained Rayleigh wave group velocity distribution at 0.1 s period together with the trace of the head scarp is shown in Fig. 9a. The stable block is situated west of the scarp.

According to the checkerboard tests, the resolution is best in the central part of the studied area where ray coverage is dense (Fig. 8). The smallest resolvable anomaly size is around 20×20 m. Along the head scarp the resolution can be considered satisfactory. However, close to the edge the ray coverage and consequently the checkerboard pattern recovery is poor, thus interpretation must be made with caution. Furthermore, based on these tests the amplitude of an anomaly cannot be well determined, which is expected as usually calculated anomalies are lower than true anomalies (Rawlinson et al, 2014). Despite that, it is possible to reliably obtain the signs (positive or negative) of the anomalies compared to the average group velocity of the studied area.

We determined the standard deviation of the resulting velocities by the bootstrapping method (Fig. 9b). The median error value for the studied area is 15 ms^{-1}. On the majority of the area the standard deviation is less than 20 ms^{-1}, the highest values (30–40 ms^{-1}) can be found at a low velocity anomaly. These error values confirm the reliability of the estimated Rayleigh wave group velocity pattern even in the low velocity area.

Based on the SNR values illustrated in Fig. 5, we have summarised the directionality information as shown in the figure inset and found that noise sources contributing to the cross-correlation function with the highest SNR are located in the direction of the residential area of Dunaszekcső. The Danube can be considered as one of the main local noise sources, however, it flows approximately 60 m below the studied area, therefore the examined surface waves cannot presumably be gen-

erated by the Danube. Our directionality analysis confirms this assumption.

Several authors have argued about the effect of non-uniform noise source distribution on the cross-correlation function and lag time. Based on theoretical considerations Tsai (2009) has shown that non-uniform noise source distribution can cause a few percent error in lag time, however Yang and Ritzwoller (2008) have also shown that even when the majority of the sources are clustered the traveltime estimate can be stable due to the azimuthally evenly distributed less energetic noise sources. Although the number of cross-correlation functions of our study is relatively low and noise source directivity is present, Fig. 5 shows that noise sources with varying energy can be found in every direction, therefore the cross-correlation function is probably adequate for group velocity measurements. In addition, in the presented study the obtained velocity anomalies are in the order of several 10 percent, which is much larger than the potential effect of anisotropic noise source distribution estimated by Tsai (2009). These suggest that the obtained group velocity pattern can be considered reliable.

Azimuthally dependent velocities would emerge either from non-uniform noise source distribution or from anisotropy at the study area. Therefore azimuth versus group velocity and traveltimes as a function of the distance and the azimuth between each station pair were plotted (Fig. 7). In spite of the high possibility of anisotropy, Fig. 7 does not show clear azimuthal dependence of velocities, possibly due to the relatively low number of data. Anisotropy is most likely to occur around the northern end of the head scarp, however, only a few short paths were measured in this area, therefore this might be the reason for not detecting it.

We found the average Rayleigh wave group velocity to be 171 ms^{-1} at 0.1 s period. Using the previously mentioned homogeneous half space approximation (cf. section 6) the Rayleigh wave velocity is slightly less than the shear velocity, therefore the determined average group velocity is consistent with the shear wave velocities measured in near surface loess sequences located at other parts of the world (e.g. v_S=192±37 ms^{-1} in Gomberg et al (2003)).

The group velocity distribution shows that the studied area can be divided into two regions. The northeastern part is characterised by relatively low velocities, while the southwestern part by higher velocities. Along most of the head scarp negative anomaly can be seen, in the northern section the anomaly is wide, its width reaches 30-40 m. It is noteworthy that the axis of the negative anomaly do not coincide with the trace of the head scarp. According to the checkerboard tests, the recovered anomaly pattern is distorted here, therefore it can not be excluded that the shape of the anomaly reflects the shortcomings of the resolution. At the southern part of the scarp, the negative anomaly is less widespread with smaller amplitude, it affects only a narrow area. At the northernmost part of the scarp a positive anomaly is visible, however this is at the edge of the study area, where the results are less reliable and its size is also less than the smallest resolvable detail.

An abandoned house is located at the eastern edge of the study area, at approximate local coordinates x=90 m and y=20 m. It is possible that the weak, positive anomaly that appears there reflects the effect of this house's foundation.

At the northwestern part of the study area a smaller low velocity anomaly can be seen, which might indicate a previously unknown loosened domain.

The southwestern part of the study area shows higher than average velocities. The location of the highest velocities more or less coincides with the presumable location of the remnants of the fortresses at the Castle Hill. They might be caused by the buried remnants of the walls or rock debris resulting either from sieges or from demolition carried out by the local population. The resolution of the presented tomographic map is much less than the supposed wall thicknesses, therefore a detailed geophysical survey is needed to understand the revealed velocity distribution.

Based on the previous geotechnical and geomorphological investigations (e.g. Moyzes and Scheuer, 1978), the composition of the upper few tens of metres of the loess bluff can be considered homogeneous both vertically and laterally compared to either the used grid spacing or the occurring wavelengths. Therefore we suppose that the revealed low velocity anomalies are associated with tension cracks. The lowest velocities represent highly creviced areas, which can be seen on the surface as approximately 20–40 cm wide cracks. According to the field observations, slope failure initiates at the northern part of the head scarp, where failure process affects a several meter wide area (Fig. 1).

8 Conclusions

The active landslide at Castle Hill has been studied by geomorphological geotechnical, geodetical and geoelectrical methods in the last decades, however, seismic tomographic imaging of the study area was lacking. We applied ambient noise tomography to determine Rayleigh wave group velocities.

The study site is a loess high bank which lies approximately 60 m above the average water level of the

Danube. Due to the topography and the proximity of the river and the residential area, the criterion of uniform noise source distribution for seismic interferometry was not satisfied. Despite that, the noise correlation method was successfully used at engineering-geotechnical scale. The directionality analysis has shown that noise sources contributing to the cross-correlation function with the highest SNR are located in the direction of the residential area.

The effect of non-uniform noise source distribution can be similar to that of anisotropy, both could give rise to azimuth dependent velocities. Despite the revealed directionality of noise sources, neither the plot of azimuth versus group velocity (Fig. 7a) nor the plot of delay times as a function of distance and azimuth between each station pair (Fig. 7b) show clear azimuthal dependence, thus anisotropy could not be observed.

We applied phase cross-correlation and time-frequency phase weighted stacking to obtain the cross-correlation functions. The derived dispersion curves were almost flat in the 0.05–0.2 s period range, therefore depth-velocity inversion was not carried out. However, the lack of dispersion indicates a vertically homogeneous near surface medium.

Tomographic computations were carried out to determine the Rayleigh wave group velocity distribution. We estimated the resolution by checkerboard tests and the error bounds for the velocity values by bootstrap analysis. The velocity distribution is well constrained at the central part of the study area and the resolution is less satisfactory around the head scarp, but still allows careful interpretation.

The average Rayleigh wave group velocity at the loess sequence of the Castle Hill was found to be 171 ms^{-1}, which is consistent with measured shear wave velocities in near surface loess sequences (e.g. Gomberg et al, 2003; Havenith et al, 2007). The median error value determined by bootstrap analysis is 15 ms^{-1}, the highest values of 30-40 ms^{-1} can be found at the northern part of the head scarp (Fig. 9).

We have identified a low-velocity region, which represents a highly creviced area, where tension cracks are visible at the surface and the slope failure takes place along a wide area. Another low velocity region was found at the northwestern part of the study area as well, which might indicate a previously unknown, loosened domain.

The highest velocities were observed at the supposed remnants of the historical fort, however due to the lack of archaeological excavations a detailed geophysical survey including other geophysical methods is needed in order to reveal the source of the high velocity anomaly.

This study confirms the results of e.g. Renalier et al (2010) and Pilz et al (2014), according to which the ambient noise cross-correlation method can be useful in the characterisation of landslides. Low Rayleigh wave group velocity zones were partially explainable with known near-surface features, showing that ambient noise tomography is suitable for detecting creviced areas at a high bank. We have found a previously unknown low velocity region as well. The results suggest that in the future it will be possible to map those locations at other bluffs along the Danube which are most prone to slide.

Acknowledgements We are grateful to Prof. Zsolt Visy for his help in the archaeological characterisation of the investigated area and to Katalin Gribovszki for the site's digital elevation model. We express our thanks to the colleagues who helped organising the measurements and participated in them. We thank Dr. Yannik Behr and an anonymous reviewer for their constructive comments on the manuscript, the quality of the revised paper has been improved significantly thanks to their remarks and suggestions. Processing of the measured data was carried out using the Python software package ObsPy (Beyreuther et al, 2010). Maps and plots were prepared using Generic Mapping Tools (Wessel et al, 2013). This study was supported by the Hungarian Scientific Research Fund under Grant OTKA K105399 and K81295. The travel of Zdeněk Kaláb and Markéta Lednická was supported by the bilateral project between the Institute of Geonics (Ostrava) and the MTA Kövesligethy Radó Seismological Observatory (Budapest) (NKM30/2015).

References

Ammon CJ (2001) Notes on Seismic Surface-Wave Processing Part I: Group Velocity Estimation. Saint Louis University

Bányai L, Mentes Gy, Újvári G, Kovács M, Czap Z, Gribovszki K, Papp G (2014) Recurrent landsliding of a high bank at Dunaszekcső, Hungary: geodetic deformation monitoring and finite element modeling. Geomorphology 210:1–13, DOI 10.1016/j.geomorph.2013.11.032

Barmin M, Ritzwoller M, Levshin A (2001) A fast and reliable method for surface wave tomography. In: Monitoring the Comprehensive Nuclear-Test-Ban Treaty: Surface Waves, Springer, pp 1351–1375, DOI 10.1007/978-3-0348-8264-4_3

Barton N (2007) Rock quality, seismic velocity, attenuation and anisotropy. Taylor&Francis

Bensen G, Ritzwoller M, Yang Y (2009) A 3-D shear velocity model of the crust and uppermost mantle beneath the United States from ambient seismic noise. Geophysical Journal International 177(3):1177–1196, DOI 10.1111/j.1365-246X.2009.04125.x

Bensen GD, Ritzwoller MH, Barmin MP, Levshin AL, Lin F, Moschetti MP, Shapiro NM, Yang

Y (2007) Processing seismic ambient noise data to obtain reliable broad-band surface wave dispersion measurements. Geophysical Journal International 169(3):1239–1260, DOI 10.1111/j.1365-246X.2007.03374.x

Beyreuther M, Barsch R, Krischer L, Megies T, Behr Y, Wassermann J (2010) Obspy: A python toolbox for seismology. Seismological Research Letters 81(3):530–533, DOI 10.1785/gssrl.81.3.530

Bijwaard H, Spakman W, Engdahl ER (1998) Closing the gap between regional and global travel time tomography. Journal of Geophysical Research: Solid Earth 103(B12):30,055–30,078, DOI 10.1029/98JB02467

Bugya T, Fábián SÁ, Görcs NL, Kovács IP, Radvánszky B (2011) Surface changes on a landslide affected high bluff in Dunaszekcső (Hungary). Central European Journal of Geosciences 3(2):119–128, DOI 10.2478/s13533-011-0014-6

Campillo M, Paul A (2003) Long-Range Correlations in the Diffuse Seismic Coda. Science 299(5606):547–549, DOI 10.1126/science.1078551

Cho K, Herrmann R, Ammon C, Lee K (2007) Imaging the upper crust of the Korean Peninsula by surface-wave tomography. Bulletin of the Seismological Society of America 97(1B):198–207, DOI 10.1785/0120060096

Danneels G, Bourdeau C, Torgoev I, Havenith HB (2008) Geophysical investigation and dynamic modelling of unstable slopes: case-study of Kainama (Kyrgyzstan). Geophysical Journal International 175(1):17–34, DOI 10.1111/j.1365-246X.2008.03873.x

De Nisco G, Nunziata C (2011) V_S Profiles from Noise Cross Correlation at Local and Small Scale. Pure and Applied Geophysics 168(3-4):509–520, DOI 10.1007/s00024-010-0119-8

Dias RC, Julià J, Schimmel M (2015) Rayleigh-wave, Group-Velocity Tomography of the Borborema Province, NE Brazil, from Ambient Seismic Noise. Pure and Applied Geophysics 172(6):1429–1449, DOI 10.1007/s00024-014-0982-9

Dziewonski A, Bloch S, Landisman M (1969) A technique for the analysis of transient seismic signals. Bulletin of the Seismological Society of America 59:427–444

Efron B (1979) Computers and the theory of statistics: thinking the unthinkable. Siam Review 21(4):460–480, DOI 10.1137/1021092

Gergova D, Iliev I, Rizzo V (1995) Evidence of a seismic event on Thracian tombs dated to the Hellenistic period (Sveshtari, Northeastern Bulgaria). Annals of Geophysics 38(5-6), DOI 10.4401/ag-4089

Gomberg J, Waldron B, Schweig E, Hwang H, Webbers A, VanArsdale R, Tucker K, Williams R, Street R, Mayne P, et al (2003) Lithology and Shear-Wave Velocity in Memphis, Tennessee. Bulletin of the Seismological Society of America 93(3):986–997, DOI 10.1785/0120020164

Gorbatikov A, Kalinina A, Volkov V, Arnoso J, Vieira R, Velez E (2004) Results of analysis of the data of microseismic survey at Lanzarote Island, Canary, Spain. In: Geodetic and Geophysical Effects Associated with Seismic and Volcanic Hazards, Springer, pp 1561–1578, DOI 10.1007/978-3-0348-7897-5_17

Gouedard P, Stehly L, Brenguier F, Campillo M, Colin de Verdiere Y, Larose E, Margerin L, Roux P, Sánchez-Sesma FJ, Shapiro N, et al (2008) Cross-correlation of random fields: Mathematical approach and applications. Geophysical prospecting 56(3):375–393, DOI 10.1111/j.1365-2478.2007.00684.x

Havenith HB, Fäh D, Polom U, Roullé A (2007) S-wave velocity measurements applied to the seismic microzonation of Basel, Upper Rhine Graben. Geophysical Journal International 170(1):346–358, DOI 10.1111/j.1365-246X.2007.03422.x

Hegedűs E (2008) A megcsúszott dunaszekcsői löszfal aktív és passzív szeizmikus vizsgálata (Active and passive seismic investigation of the slipped loess bluff at Dunaszekcső). Tech. rep., Eötvös Loránd Geofizikai Intézet

Herrmann R (1973) Some aspects of band-pass filtering of surface waves. Bulletin of the Seismological Society of America 63(2):663

Herrmann RB, Ammon CJ (2002) Computer Programs in Seismology: Surface Waves, Receiver Functions and Crustal Structure. Saint Louis University, Missouri

Hofmann-Wellenhof B, Lichtenegger H, Collins J (2001) Global Positioning System: theory and practice. Springer-Verlag, New York, DOI 10.1007/978-3-7091-6199-9

Kovács IP, Fábián SÁ, Radvánszky B, Varga G (2015) Dunaszekcső Castle Hill: Landslides Along the Danubian Loess Bluff. In: Landscapes and Landforms of Hungary, Springer, pp 113–120, DOI 10.1007/978-3-319-08997-3_14

Kraft J (2011) Dunai magaspart dunaszekcsői részletének rogyásos suvadásai (Slumping of Danube's high bank at Dunaszekcső). Mérnökgeológia-Kőzetmechanika pp 93–104

Lay T, Wallace TC (1995) Modern Global Seismology. Academic press

Lévěque JJ, Rivera L, Wittlinger G (1993) On the use of the checker-board test to assess the resolution of tomographic inversions. Geophysical Journal

International 115(1):313–318, DOI 10.1111/j.1365-246X.1993.tb05605.x

Levshin A, Yanovskaya T, Lander A, Bukchin B, Barmin M, Ratnikova L, Its E (1989) Seismic Surface Waves in a Laterally Inhomogeneous Earth, Modern Approaches in Geophysics, vol 9. Kluwer Academic Puhlishers, Dordrecht, DOI 10.1007/978-94-009-0883-3

Lin FC, Ritzwoller MH, Townend J, Bannister S, Savage MK (2007) Ambient noise Rayleigh wave tomography of New Zealand. Geophysical Journal International 170(2):649–666, DOI 10.1111/j.1365-246X.2007.03414.x

Lóczy D, Balogh J, Ringer Á (1989) Landslide hazard induced by river undercutting along the Danube. Geomorphological Hazards, Supplements of Geografia Fisica e Dinamica Quaternaria 2:5–11

Luo Y, Yang Y, Xu Y, Xu H, Zhao K, Wang K (2015) On the limitations of interstation distances in ambient noise tomography. Geophysical Journal International 201(2):652–661, DOI 10.1093/gji/ggv043

Lóczy D (ed) (2015) Landscapes and Landforms of Hungary. World Geomorphological Landscapes, Springer International Publishing

Menke W (1989) Geophysical data analysis: Discrete inverse theory. International Geophysics Series, New York: Academic Press, 1989, Rev ed 1

Mentes Gy, Bányai L, Újvári G, Papp G, Gribovszki K, Bódis VB (2012) Recurring mass movements on the Danube's bank at Dunaszekcső (Hungary) observed by geodetic methods. Journal of Applied Geodesy 6(3-4):203–208, DOI 10.1515/jag-2012-0011

Moyzes A, Scheuer Gy (1978) A dunaszekcsői magaspart mérnökgeológiai vizsgálata (Engineering geological investigation of the high bank at Dunaszekcső). Földtani Közlöny 108:213–226

Nakamura Y (2000) Clear identification of fundamental idea of Nakamura's technique and its applications. In: Proceedings of the 12th world conference on earthquake engineering, p 2656

Picozzi M, Parolai S, Bindi D, Strollo A (2009) Characterization of shallow geology by high-frequency seismic noise tomography. Geophysical Journal International 176(1):164–174, DOI 10.1111/j.1365-246X.2008.03966.x

Pilz M, Parolai S, Picozzi M, Bindi D (2012) Three-dimensional shear wave velocity imaging by ambient seismic noise tomography. Geophysical Journal International 189(1):501–512, DOI 10.1111/j.1365-246X.2011.05340.x

Pilz M, Parolai S, Bindi D, Saponaro A, Abdybachaev U (2014) Combining seismic noise techniques for landslide characterization. Pure and Applied Geophysics 171(8):1729–1745, DOI 10.1007/s00024-013-0733-3

Rawlinson N, Fichtner A, Sambridge M, Young MK (2014) Chapter One - Seismic Tomography and the Assessment of Uncertainty. Advances in Geophysics, vol 55, Elsevier, pp 1 – 76, DOI 10.1016/bs.agph.2014.08.001

Ren Y, Grecu B, Stuart G, Houseman G, Hegedűs E, SCP Working Group (2013) Crustal structure of the Carpathian–Pannonian region from ambient noise tomography. Geophysical Journal International 195(2):1351–1369, DOI 10.1093/gji/ggt316

Renalier F, Jongmans D, Campillo M, Bard PY (2010) Shear wave velocity imaging of the Avignonet landslide (France) using ambient noise cross correlation. Journal of Geophysical Research: Earth Surface (2003–2012) 115(F3), DOI 10.1029/2009JF001538

Sabra KG, Gerstoft P, Fehler MC, Gerstoft P, Roux P, Kuperman WA, Kuperman WA, Fehler MC (2005a) Extracting time-domain Green's function estimates from ambient seismic noise. Geophysical Research Letters 32:L03,310, DOI 10.1029/2004GL021862

Sabra KG, Roux P, Kuperman W (2005b) Emergence rate of the time-domain green's function from the ambient noise cross-correlation function. The Journal of the Acoustical Society of America 118(6):3524–3531, DOI 10.1121/1.2109059

Schimmel M (1999) Phase cross-correlations: Design, comparisons, and applications. Bulletin of the Seismological Society of America 89(5):1366–1378

Schimmel M, Gallart J (2007) Frequency-dependent phase coherence for noise suppression in seismic array data. Journal of Geophysical Research: Solid Earth 112(B4), DOI 10.1029/2006JB004680

Schimmel M, Stutzmann E, Gallart J (2011) Using instantaneous phase coherence for signal extraction from ambient noise data at a local to a global scale. Geophysical Journal International 184(1):494–506, DOI 10.1111/j.1365-246X.2010.04861.x

Shapiro NM, Campillo M (2004) Emergence of broadband Rayleigh waves from correlations of the ambient seismic noise. Geophysical Research Letters 31:5, DOI 10.1029/2004GL019491

Shapiro NM, Campillo M, Stehly L, Ritzwoller MH (2005) High-Resolution Surface-Wave Tomography from Ambient Seismic Noise. Science 307(5715):1615–1618, DOI 10.1126/science.1108339

Stankiewicz J, Weber MH, Mohsen A, Hofstetter R (2012) Dead Sea Basin imaged by ambient seismic noise tomography. Pure and Applied Geophysics 169(4):615–623, DOI 10.1007/s00024-011-0350-y

Szalai S, Szokoli K, Metwaly M (2014a) Delineation of landslide endangered areas and mapping their frac-

ture systems by the pressure probe method. Landslides 11(5):923–932, DOI 10.1007/s10346-014-0509-6

Szalai S, Szokoli K, Novák A, Tóth Á, Metwaly M, Prácser E (2014b) Fracture network characterisation of a landslide by electrical resistivity tomography. Natural Hazards and Earth System Sciences Discussions 2(6):3965–4010, DOI 10.5194/nhessd-2-3965-2014

Szanyi Gy, Gráczer Z, Győri E (2013) Ambient seismic noise Rayleigh wave tomography for the Pannonian basin. Acta Geodaetica et Geophysica 48(2):209–220, DOI 10.1007/s40328-013-0019-3

Tichelaar BW, Ruff LJ (1989) How good are our best models? Jackknifing, bootstrapping, and earthquake depth. Eos, Transactions American Geophysical Union 70(20):593–606, DOI 10.1029/89EO00156

Tsai VC (2009) On establishing the accuracy of noise tomography travel-time measurements in a realistic medium. Geophysical Journal International 178(3):1555–1564, DOI 10.1111/j.1365-246X.2009.04239.x

Újvári G, Mentes Gy, Bányai L, Kraft J, Gyimóthy A, Kovács J (2009) Evolution of a bank failure along the River Danube at Dunaszekcső, Hungary. Geomorphology 109(3-4):197–209, DOI 10.1016/j.geomorph.2009.03.002

Visy Z (2003) The Ripa Pannonica in Hungary. Akadémiai Kiadó

Wang L, Wu Z, Chen T (2012) Study on the Site Effects on Ground Motion during the Wenchun Ms8.0 Earthquake, China. Lisbon, Portugal, Proceeding of the fifteenth World Conference on Earthquake Engineering, pp 1–10

Wessel P, Smith WH, Scharroo R, Luis J, Wobbe F (2013) Generic Mapping Tools: Improved Version Released. EOS Transactions American Geophysical Union 94(45):409–410, DOI 10.1002/2013EO450001

Yang Y, Ritzwoller MH (2008) Characteristics of ambient seismic noise as a source for surface wave tomography. Geochemistry, Geophysics, Geosystems 9(2), DOI 10.1029/2007GC001814

Yang Y, Ritzwoller MH, Levshin AL, Shapiro NM (2007) Ambient noise Rayleigh wave tomography across Europe. Geophysical Journal International 168(1):259–274, DOI 10.1111/j.1365-246X.2006.03203.x

Yanovskaya TB, Kizima ES, Antonova LM (1998) Structure of the crust in the Black Sea and adjoining regions from surface wave data. Journal of Seismology 2(4):303–316, DOI 10.1023/A:1009716017960